Journal of Solid State Chemistry **146,** 103–109 (1999)
Article ID jssc.1999.8314, available online at http://www.idealibrary.com on IDEAL®

The $\delta \rightarrow \varepsilon \rightarrow \gamma$ LiV_2O_5 "High Temperature" Phase Transitions Evidenced by Synchrotron X-Ray Powder Diffraction Analysis

Christine Satto,* Philippe Sciau,* Eric Dooryhee,† Jean Galy,* and Patrice Millet*,[1]

*Centre d'Elaboration de Matériaux et d'Etudes Structurales, CNRS, 29 rue Jeanne Marvig, BP 4347, 31055 Toulouse Cedex, France; and †European Synchrotron Radiation Facility (ESRF), BP 220, F-38043, Grenoble Cedex, France

Received October 29, 1998; in revised form March 24, 1999; accepted April 8, 1999

The structural evolution and the temperature ranges of stability for the δ, ε, and γ phases of the lithium vanadium oxide bronze LiV_2O_5 are evidenced by use of synchrotron X-ray powder diffraction in the temperature range 100–250°C. It is shown that δ-LiV_2O_5 is stable below 120°C and that the complete transformation to the high temperature form γ-LiV_2O_5 is achieved above 220°C. In the temperature range 120–220°C ε-LiV_2O_5 is the stable polymorph. The temperature dependence of the cell parameters for the phase δ- and γ-LiV_2O_5 are measured and the crystal structure of ε-LiV_2O_5 has been determined using the Rietveld method. It crystallizes in the orthorhombic system and at 140°C the cell parameters are $a = 11.3552(6)$ Å, $b = 3.5732(2)$ Å, and $c = 4.6548(3)$ Å. Arguments supporting the choice of the space group *Pmmn,* as for another bronze α' NaV_2O_5, are given.

INTRODUCTION

The suitability of the V_2O_5 structure for insertion reactions was recognized in the sixties when vanadium bronzes were intensively studied. In particular, a lot of work was devoted to the $Li_xV_2O_5$ system due to the possible application as positive electrode materials for secondary batteries. More recently the room temperature phase diagram of $Li_xV_2O_5$ for $0 \leq x \leq 1$ was reported by Murphy *et al.* (1) and Dickens *et al.* (2). Three single-phase regions were identified: α $Li_xV_2O_5$ for $0 < x < 0.13$, ε $Li_xV_2O_5$ for $0.32 < x < 0.80$, and δ $Li_xV_2O_5$ for $0.88 < x < 1.00$. Recently, it has been shown that the ε range is not single-phased (3–5), but is composed of two kinds of incommensurately modulated structures called $\varepsilon 1$ for $0.32 \leq x \leq 0.55$ and $\varepsilon 2$ for $0.55 \leq x \leq 0.80$ (4). Furthermore a structural model has been proposed for the incommensurate phase $\varepsilon 1$ $Li_xV_2O_5$ with $x = 0.4$; the perturbation of the periodic structure is a result of an incommensurate ordering of the Li^+ ions (6).

This study is focused on the highest value of x, corresponding to the δ $Li_xV_2O_5$ phase, i.e, $x = 1$. The structure of δ LiV_2O_5 determined by powder neutron diffraction techniques by Cava *et al.* (7) and recently refined from X-ray powder diffraction data by Rietveld analysis (8) shows an atomic arrangement with $[V_2O_5]_n$ single layers alternatively shifted by $a/2$ along the [100] direction (space group *Cmcm*). The aim of this paper is to describe the structural evolution of δ LiV_2O_5 upon heating. For this purpose, we performed synchrotron X-ray powder diffraction analysis of the $\delta \rightarrow \varepsilon \rightarrow \gamma$ LiV_2O_5 phase transitions, γ LiV_2O_5 being the high temperature form (9). In addition to the evolution of the lattice parameter for the different phases we report a structure refinement of the high lithium containing ε phase formed. Deramond (10) recorded powder X-ray diffraction patterns after heating δ LiV_2O_5 under vacuum, but did not obtain pure ε LiV_2O_5; the γ phase appeared after a thermal treatment at a temperature as low as 110°C. The present work allows us to propose a description of the phase diagram of this interesting class of compounds.

EXPERIMENTAL

δ $Li_xV_2O_5$, with $0.95 \leq x \leq 1$, was prepared by soft chemistry, V_2O_5 being reduced with the appropriate amount of lithium iodide in acetonitrile. The resulting mixture was stirred for 24 h at room temperature under argon. The color of the powder changed from orange to dark blue. The compound isolated by filtration was washed under argon with first acetonitrile and then acetone and finally dried under vacuum for 24 h.

Synchrotron radiation powder diffraction data were collected on the beam line BM 16 of the European Synchrotron Radiation Facility (ESRF) situated in Grenoble. The powder was sealed in a 1 mm diameter borosilicate glass capillary mounted on a spinning holder on the axis of the diffractometer in order to minimize the effect of preferred orientation. Data were collected using a Si(111) monochromator and the detector consisted of a nine-channel

[1]To whom correspondence should be addressed.

0022-4596/99 $30.00

multianalyser stage (Ge(111)) with a separation of two degrees between each channel. The channel counts were summed up and rebinned, taking into account the different detector efficiencies and the decay of the beam current during the scan, to produce the equivalent normalized step scan. The capillaries were heated up by a stream of hot air. Three kinds of measurement were performed at a wavelength of 0.64667 Å: (i) a study of the phase transformations $\delta \rightarrow \varepsilon \rightarrow \gamma$ with increasing temperature, (ii) a precise recording of the diffractogram of the ε LiV_2O_5 phase at 140°C, and (iii) dynamic measurements with a temperature ramp of 0.5°C/min applied to the sample from 100 to 240°C. The acquisition time was 3 min per pattern with a dead time of 7 min between two successive measurements. This enabled the recording of diffractogram over 23° in 2θ every 5°C with a temperature variation of only 1.5°C during each measurement. The detector assembly was scanned from 5 to 23° in 2θ at 0.83°/min. For the static measurement, data were collected in a number of successive scans between 5 and 50° in 2θ at a rate of 0.25°/min. The number of scans was increased between 30 and 50° in 2θ in order to improve the statistics and compensate for the normal fall-off of the scattering power at higher angles. The recording conditions are summarized in Table 1.

TABLE 1
Experimental Conditions for the Structural Determination of ε LiV_2O_5

Data collection		
Beam line	BM 16	
Instrument geometry	Transmission	
Monochromator	Si(1 1 1)	
Detector	nine-channel multianalyser stage (Ge(1 1 1))	
Wavelength (Å)	0.64667	
2θ range (°)	5–50	
Scan rate	0.25° 2θ/min	
$(\sin\theta)/\lambda_{max}$ ($Å^{-1}$)	0.65	
Maximum counts	37500	
Average background	400	
Temperture (°C)	140 (2)	
Refinement		
Refinement on weighting scheme		$S = \sum w_i(Y_{Oi} - Y_{Ci})^2$ $w = 1/\sigma^2(I)$
Analytical function for profile		Pseudo-Voigt
Asymmetry correction		4 parameters
Absorption correction (μR)		0.8
R-factors $R_{wp} = \sqrt{\frac{\sum w_i(Y_{oi} - Y_{ci})^2}{\sum w_i(Y_{oi})^2}}$		$R_{Bragg} = \frac{\sum\lvert I_o - I_c\rvert}{\sum I_o}$
$R_{exp} = \sqrt{\frac{(N_o - P)}{\sum w_i(Y_{oi})^2}}$		
Computer program		XND 1.12 (Bérar)

RESULTS

The structural evolutions of the X-ray powder patterns of δ LiV_2O_5 on heating are summarized in Fig. 1. For clarity, the main peaks of the δ, ε, and γ phases are indexed. As can be seen, the starting compound consists mainly of the δ phase and a small amount of ε $Li_xV_2O_5$. The temperature evolution of the intensity of the main peak of each phase is presented in Fig. 2. This allows identification of the temperature range where the phases are stable upon heating. The transformation $\delta \rightarrow \varepsilon$ begins around 110°C and ends at around 130°C. The $\varepsilon \rightarrow \gamma$ transformation takes place between 175 and 220°C and it is necessary to heat above 235°C to obtain a complete transformation of ε into γ $Li_xV_2O_5$. Once formed, γ $Li_xV_2O_5$ is stable. The unit cell parameters of the three phases were least squares refined and the results are reported in Fig. 3. The cell parameters of the starting and the final compounds, δ $Li_xV_2O_5$ (space group *Amam*) and γ $Li_xV_2O_5$ (space group *Pnma*) are, respectively, $a_\delta = 11.2577(7)$ Å, $b_\delta = 3.6061(3)$ Å, and $c_\delta = 9.942(1)$ Å at 100°C and $a_\gamma = 10.714(3)$ Å, $b_\gamma = 3.615(1)$ Å, and $c_\gamma = 9.727(2)$ Å at 220°C. The cell parameter evolution clearly shows the temperature range where the ε phase is stable and the two phase regions. It is worth mentioning that in these regions the two phases are simultaneously present in the same particle and that their cell parameters have to adjust. This is highlighted by the noticeable change of slope of the cell parameter evolutions and the e.s.d.'s increase relative to at least the parameters of the minority phase. It is clear that kinetics play a major role in these tranformations and that a slower heating rate could decrease the temperature range for the two phase regions.

STRUCTURAL DESCRIPTION OF ε LiV_2O_5

The Rietveld structural determination of ε at 140°C from powder X-ray data for 1 Li per V_2O_5 has been performed using the XND program (12). The observed and difference profiles are plotted in Fig. 4. The lattice parameters are $a = 11.3552(6)$ Å, $b = 3.5732(2)$ Å, and $c = 4.6548(3)$ Å. The structure of ε LiV_2O_5 at 140°C is closely related to that of V_2O_5 (13). It is formed by layers built of VO_5 pyramids sharing edges along [010] and corners along [100], the layers being stacked along [001]. Lithium ions intercalation in V_2O_5 leads to the increase of the c parameter and the decrease of a as a result of the puckering effect. The possibility of a monoclinic distortion, occurring in the $\varepsilon 2$ phase, has been tested, but we did not observe any splitting or widening of the peaks concerned. Therefore, three orthorhombic space groups have been considered, *Pmmn*, $P2_1mn$ and $Pm2_1n$. The comparison of the agreement factors and the number of parameters used in the refinement are given in Table 2 for each space group. For the *Pmmn* and $Pm2_1n$ space groups there is only one crystallographic site for

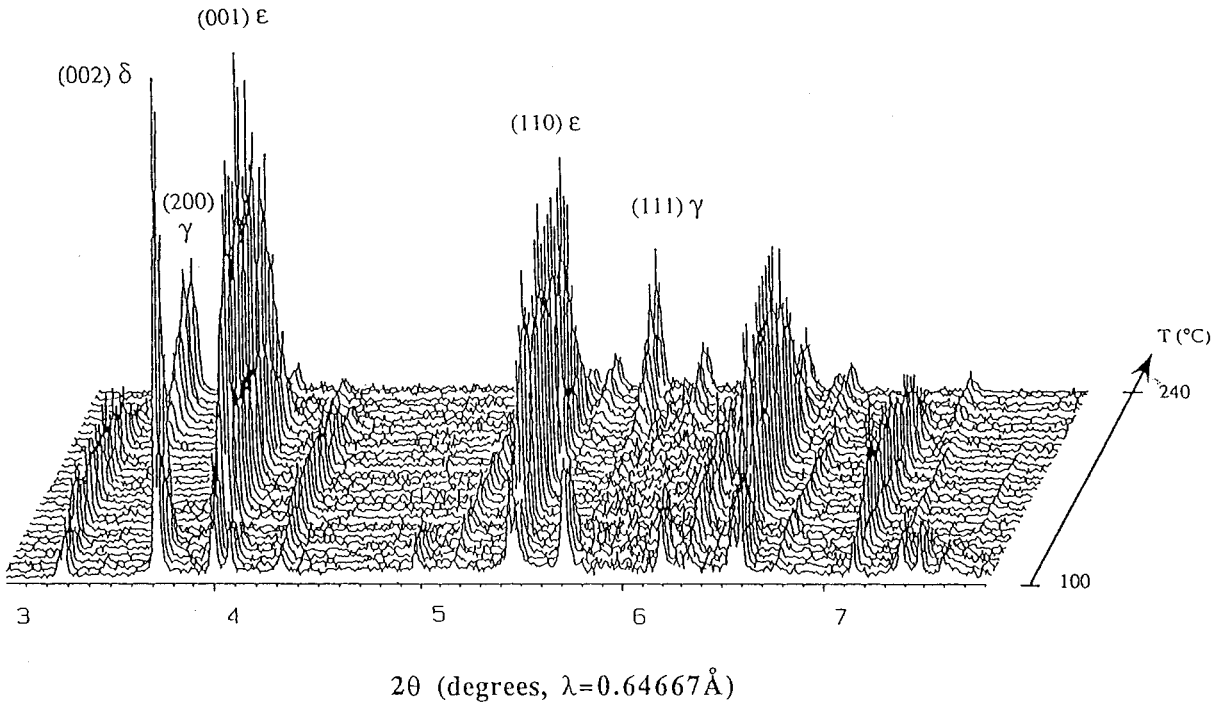

FIG. 1. X-ray powder patterns evolution of LiV_2O_5 versus temperature (representation using the program Relief (11)).

vanadium whereas for the $P2_1mn$ space group, the suppression of the mirror plane normal to a leads to the differentiation of two crystallographic sites for the vanadium atoms which could permit a separation of V^{4+} and V^{5+}. The comparison of the final atomic parameters for the two most plausible space groups *Pmmn* and $P2_1mn$ are presented in Table 3. The vanadium atoms, in both cases, are located in a square pyramid (SP). The interatomic distances are reported in Table 4. The value of the average V–O distance in the *Pmmn* space group is 1.85 Å; the same mean value is obtained in the case of δ LiV_2O_5 where no electronic localization occurs (8). In the case of the space group $P2_1mn$ the average V–O distances are 1.904 and 1.802 Å, in agreement with, respectively, $[V^{4+}O_5]$ and $[V^{5+}O_5]$ square pyramids of widely different sizes (8). However, it is worth mentioning that this differentiation could be the result of an artefact of the refinement as it has already been observed in the case of a similar compound α' NaV_2O_5 (14) where recent results indicate that the space group was in fact the centrosymmetric *Pmmn* (15) as for the α $Li_xV_2O_5$ structure type phase (16). In addition, taking into account the higher number of parameters, the slightly lower R values obtained in the noncentrosymmetric space group lead us to assume that this structure is probably centrosymmetric. The Li atom is surrounded by eight oxygen atoms forming a distorted bicaped trigonal prism. This is the same environment encountered for Na in α' NaV_2O_5; the smaller ionic radius of Li leads to a decrease of the c parameter (4.655 Å compared to 4.797 Å in α' NaV_2O_5) and a higher puckering angle of the vanadium-oxygen layer (puckering angle $\mu = 7.1°$ for ε LiV_2O_5 and $\mu = 3.2°$ for α' NaV_2O_5).

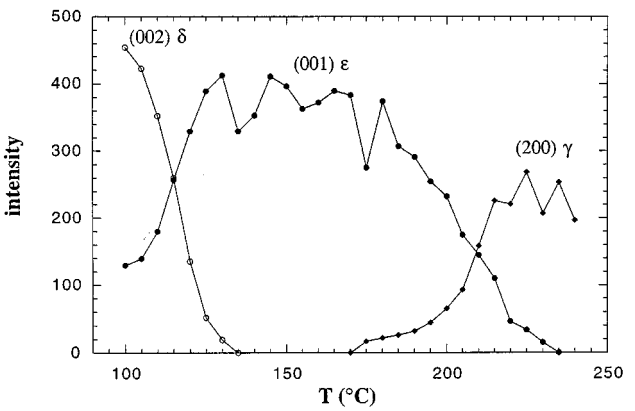

FIG. 2. Intensity variation of the main peak of the phases δ, ε, and γ LiV_2O_5.

DISCUSSION AND CONCLUSION

To our knowledge the $\delta \rightarrow \varepsilon$ and $\varepsilon \rightarrow \gamma$ transitions have never been clearly identified in $Li_xV_2O_5$ for x close to 1. The $Li_xV_2O_5$ system has been thouroughly reinvestigated by Rozier *et al.* (5). In the $0 \leq x \leq 1$ composition range, they showed that the homogeneity domain of the ε phase corres-

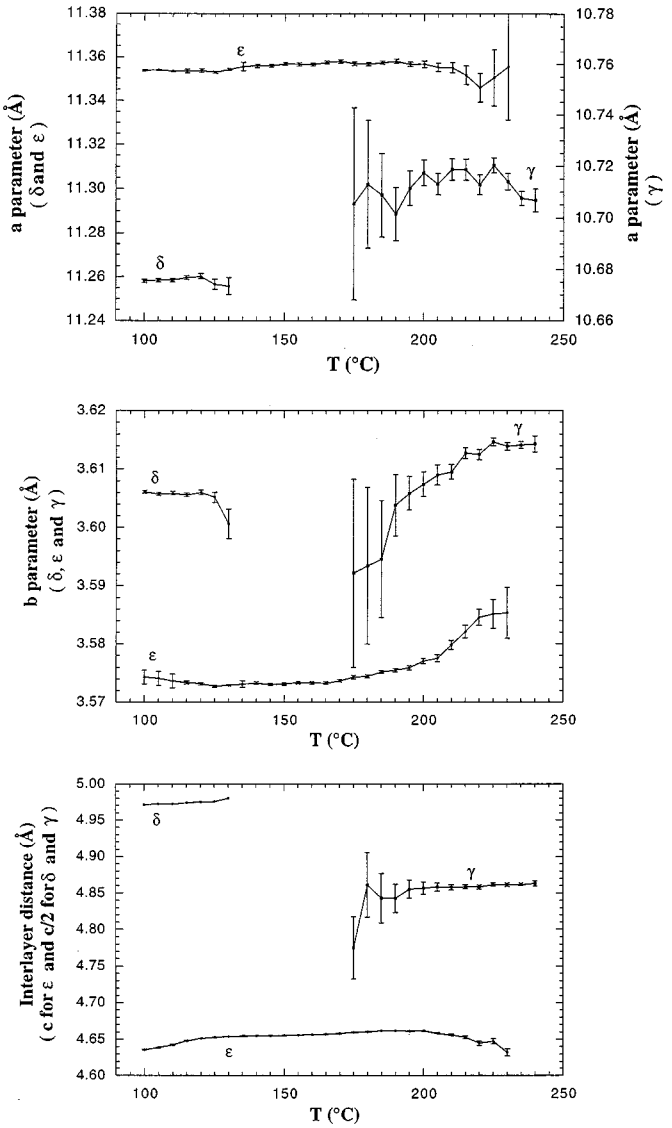

FIG. 3. Unit cell parameters evolution of the phases δ, ε, and γ LiV_2O_5 versus temperature (for clarity $c/2$ is plotted for the phases δ and γ LiV_2O_5). The estimated standard deviations are reported by bars.

ponds in fact to two successive phases, $\varepsilon 1$ and $\varepsilon 2$, both with lithium intercalating into V_2O_5 type structure with orthorhombic and monoclinic symmetries, respectively, and both incommensurate. This fact was clearly established from the evolution of the cell parameter a versus the lithium content x (Fig. 5a), by a change in slope around $x = 0.55$. Interestingly, placing on this curve the values of a (δ LiV_2O_5) and a (ε LiV_2O_5) found in this study, we observe that a (ε LiV_2O_5) lies on the straight line corresponding to the evolution of the cell parameter of a ($\varepsilon 1$ $Li_xV_2O_5$) which means that the ε phase described in this work is of the $\varepsilon 1$ type. However, it is difficult to compare our structural results in the absence of a precise structural determination of the

TABLE 2
Comparison of the Agreement Factors and the Number of Parameters for the Space Groups *Pmmn*, *Pm*2_1*n*, and *P*2_1*mn* for ε LiV_2O_5 ($T = 140°C$)

	Pmmn	*Pm*2_1*n*	*P*2_1*mn*
R_{wp}%	8.98	8.91	8.89
R_{Bragg} (%)	5.18	4.96	4.71
R_{exp} (%)	2.6	2.6	2.6
Structural parameters	13	17	21
Total parameters	46	50	54

incommensurate phases $\varepsilon 1$ $Li_xV_2O_5$. We can only conclude that the basic structure is retained. Looking at the interlayer distance c (Fig. 5b), c (ε LiV_2O_5) lies again on the straight line corresponding to c ($\varepsilon 1$ and $\varepsilon 2$ $Li_xV_2O_5$) $0.3 \leq x \leq 0.65$, $c/2$ of δ LiV_2O_5 being much bigger. Such a variation means that $\varepsilon 2$ can be seen as the early beginning of the phase transformation from ε to δ LiV_2O_5. The fact that a (δ LiV_2O_5) lies on the line corresponding to a ($\varepsilon 2$ $Li_xV_2O_5$) confirms this observation. These cell parameter evolutions

TABLE 3
Comparison of the Final Atomic Parameters in the Space Groups *Pmmn* and *P*2_1*mn* for ε LiV_2O_5 (T=140°C)

Space group	*Pmmn*	*P*2_1*mn*	
	V1	V1	V2
x	0.4002(1)	0.5999(1)	0.4004(1)
y	1/4	3/4	1/4
z	−0.1068(2)	0.1131(8)	−0.1002(8)
B_{iso} (Å^2)	0.76(2)	0.75(2)	0.75(2)
	O1	O1	O2
x	0.1193(3)	0.621(1)	0.383(1)
y	1/4	3/4	1/4
z	0.5510(7)	0.466(3)	−0.432(3)
B_{iso} (Å^2)	2.39(9)	2.3(1)	2.3(1)
	O2	O4	O5
x	0.5733(3)	0.424(1)	0.571(1)
y	1/4	3/4	1/4
z	−0.0221(6)	0.000(2)	−0.445(2)
B_{iso} (Å^2)	0.83(8)	0.49(8)	0.49(8)
	O3	O3	
x	1/4	0.254(2)	
y	1/4	1/4	
z	0.0293(9)	0.0285(9)	
B_{iso} (Å^2)	1.0(1)	0.8(1)	
	Li	Li	
x	1/4	0.218(2)	
y	3/4	3/4	
z	0.284(5)	0.280(4)	
B_{iso} (Å^2)	6.7(8)	4.1(7)	

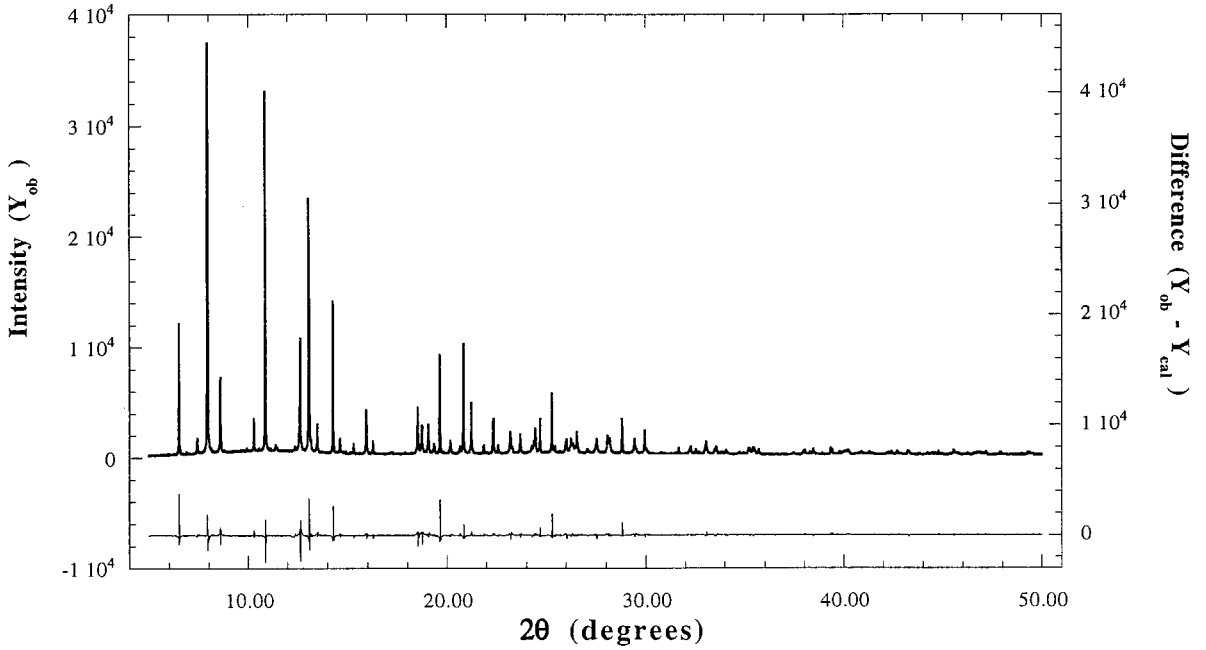

FIG. 4. Observed and difference X-ray powder pattern of ε LiV_2O_5 at 140°C. Space group *Pmmn*.

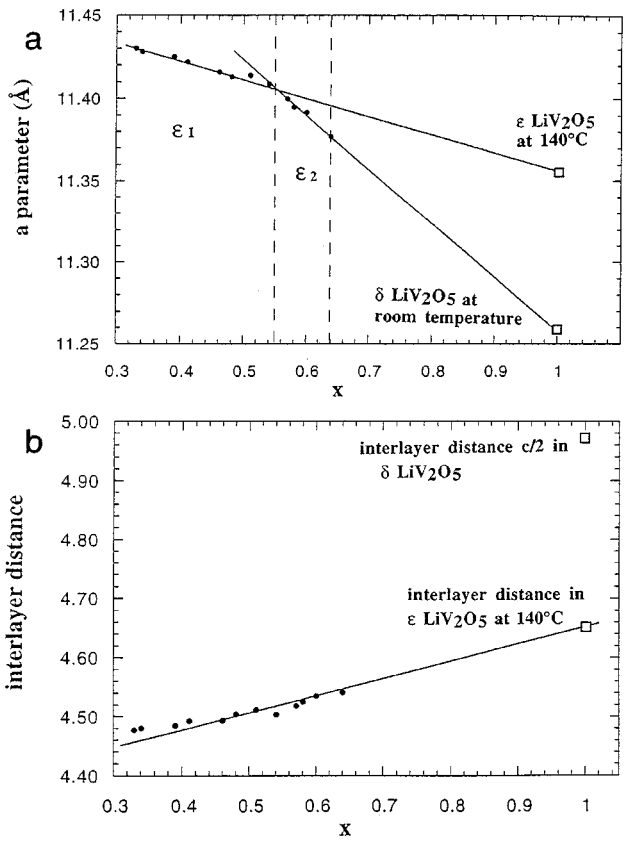

FIG. 5. Room temperture evolution of the *a* (a) and *c* (b) parameters of the ε phase as a function of the lithium content *x* from Ref. (5). The square are the values of *a* and *c* obtained in this work for ε LiV_2O_5 at 140°C and for δ LiV_2O_5 at room temperature.

are related to the structural modifications taking place when the lithium content and/or the temperature increases. Figure 6 sketches the idealized projection of the structures δ, ε, and γ viewed down the *b*-axis. At room temperature, increasing the lithium content from $x = 0.3$ up to a limit of x close to 0.7 leads to a decrease of a ($a = 11.358$ Å) which corresponds to the maximum of puckering for an ε type structure. Then to accomodate a higher lithium content, a displacement of $b/2$ of the vanadium-oxygen layer occurs leading to an interlayer distance of 4.958 Å for δ LiV_2O_5. It is worth mentioning that the lithium oxygen coordinating polyhedron changes from a trigonal prism to a tetrahedron during this transformation. Heating δ LiV_2O_5 leads to the

TABLE 4
Selected Interatomic Distances in *Pmmn* and $P2_1mn$ Space Groups

Space group	*Pmmn*			$P2_1mn$	
V–O1	1.608(3)	V1–O1	1.661(15)	V2–O2	1.558(16)
O2(×2)	1.909(1)	O5(×2)	1.960(5)	O4(×2)	1.865(4)
O2	2.005(4)	O4	2.070(15)	O5	1.955(14)
O3	1.819(2)	O3	1.869(26)	O3	1.767(26)
Mean ⟨V–O⟩	1.850		1.904		1.802
Li–O1(×4)	2.634(11)		Li–O1(×2)		2.408(18)
O2(×2)	2.348(13)		O2(×2)		2.914(21)
O3(×2)	2.144(13)		O4		2.674(25)
			O5		1.998(24)
			O3(×2)		2.176(13)

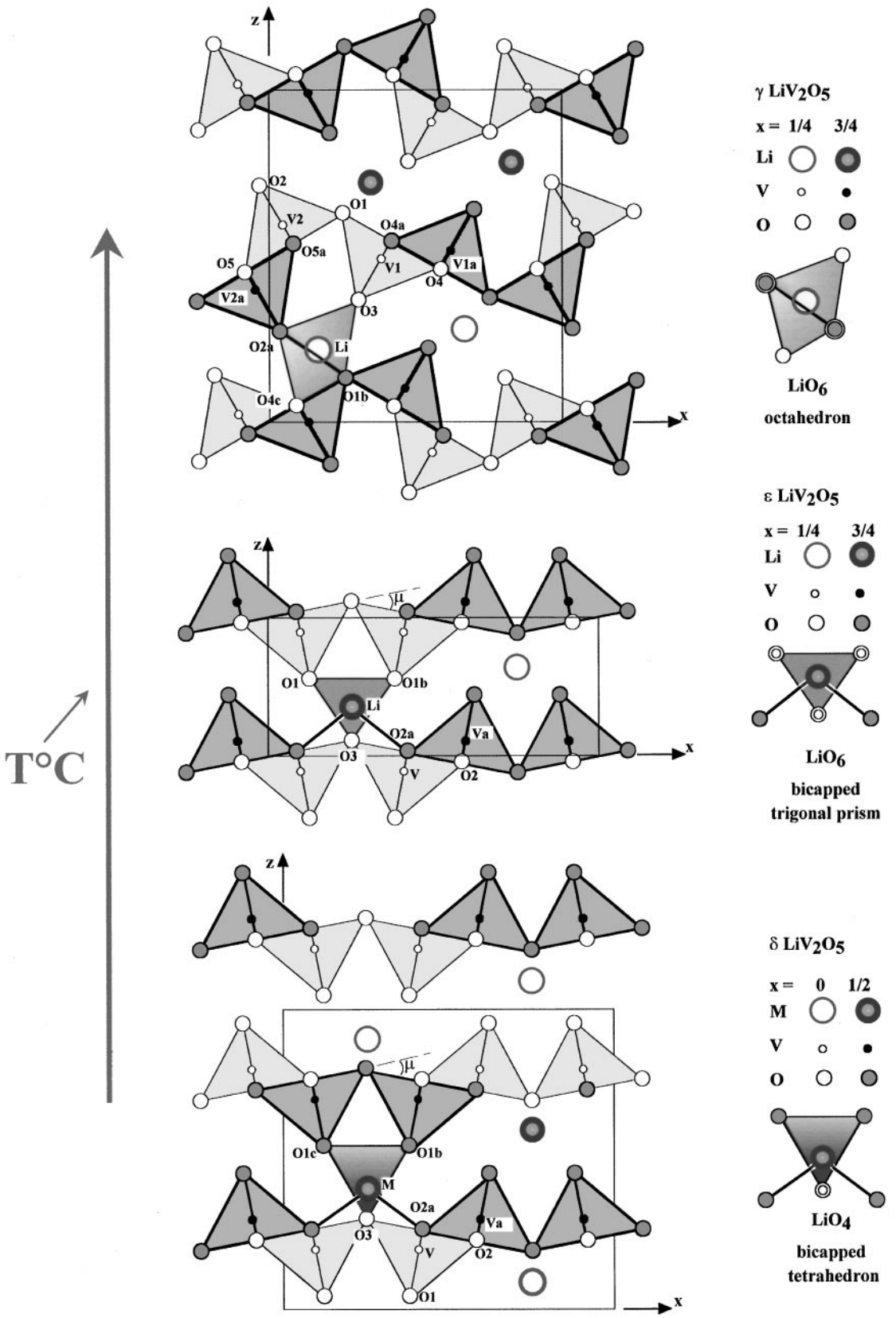

FIG. 6. Idealized projection of the δ, ε, and γ LiV_2O_5 structures viewed down the *b*-axis. For comparison, δ LiV_2O_5 is described in the nonconventional space group *Amam*.

opposite transformation ($\delta \rightarrow \varepsilon$) with the reverse $b/2$ shift of the vanadium-oxygen layer. Concerning the $\varepsilon \rightarrow \gamma$ transformation mechanism, it occurs at 220°C and can be explained by a structural mechanism already reported by Galy (17) which involves rotation of blocks of two square pyramids in order to accommodate the high value of the puckering angle observed in this structure ($\mu = 62^\circ$). As a result of this transformation the lithium atom is octahedrally coordinated by oxygen atoms.

Synchrotron X-ray powder experiments carried out at different temperatures show the existence of the $\delta \rightarrow \varepsilon \rightarrow \gamma$ LiV_2O_5 transition and allow determination of the temperature range where the ε phase is stable: 130–175°C. A structural determination of the pure ε phase obtained at 140°C shows that this compound displays the $\varepsilon 1$ $Li_xV_2O_5$ basic framework and that it is in fact isostructural with α' NaV_2O_5.

REFERENCES

1. D. W. Murphy, P. A. Christian, F. J. Disalvo, and J. V. Waszczak, *Inorg. Chem.* **18,** 2800 (1979).
2. P. G. Dickens, S. J. French, A. T. Hight, and M. F. Pye, *Mater. Res. Bull.* **14,** 1295 (1979).
3. P. Rozier, J. M. Savariault, J. Galy, J. Hirschinger, and P. Granger, *Eur. J. Solid State Chem.* **33,** 1 (1996).
4. H. Katzke, M. Czank, W. Depmeier, and S. van Smaalen, *Phil. Mag. B* **75,** 757 (1997).
5. P. Rozier, Thesis, Université Paul Sabatier, Toulouse, 1997.
6. J. M. Savariault, P. Sciau, and J. Galy, "Aperiodic'97, Proceeding of the International Conference on Aperiodic Crystals, France, August 1997," p. 347.
7. R. J. Cava, A. Santoro, D. W. Murphy, S. M. Zahurak, R. M. Fleming, P. Marsh, and R. S. Roth, *J. Solid State Chem.* **65,** 63 (1986).
8. P. Millet, C. Satto, Ph. Sciau, and J. Galy, *J. Solid State Chem.* **136,** 56 (1998).
9. J. Galy, J. Darriet, and P. Hagenmuller, *Rev. Chim. Miner.* **8,** 509 (1971).
10. E. Deramond, Thesis, Université Paul Sabatier, Toulouse, 1993.
11. B. Ducourant, B. Fraisse, and R. Fourcade, Program Relief for 3D x-ray powder patterns representation, LAMMI, Université Montpellier II, 1997.
12. J. F. Bérar and P. Garnier, APD 2nd conference, N.I.S.T. Special Pub. **846,** 212 (1992). [XND is available by anonymous ftp at ftp://labs.polycnrs-gre.fr/pub/xnd.]
13. R. Enjalbert and J. Galy, *Acta Cryst. C* **42,** 1467 (1986).
14. A. Carpy and J. Galy, *Acta Cryst. B* **31,** 1481 (1975).
15. H. G. vonSchnering, Y. Grin, M. Kaupp, M. Somer, R. K. Kremer, O. Jepsen, T. Chatterji, and M. Weiden, *Z. Krist.* **213,** 246 (1998).
16. A. Hardy, J. Galy, A. Casalot and M. Pouchard, *Bull. Soc. Chim. Fr.* **4,** 1056 (1965).
17. J. Galy, *J. Solid State Chem.* **100,** 229 (1992).